

ARTICLE OPEN



Temporal and spatial evolution of enzymatic degradation of amorphous PET plastics

Holger Lippold¹✉, Laura Kahle², Christian Sonnendecker², Jörg Matysik² and Cornelius Fischer¹

Biocatalytic degradation is an emerging strategy aiming for energy-efficient recycling of poly(ethylene terephthalate) (PET), the most commonly used thermoplastic polyester. Besides material composition and physico-chemical parameters, the degradation kinetics is co-determined by the evolving nanotopography. In this study, the 3-dimensional development of the surface characteristics of an amorphous PET film, reacted with a highly effective hydrolase enzyme for up to 24 h, was explored by vertical scanning interferometry and confocal microscopy. The spatio-temporal analysis unveiled that the degradation process is not uniform with respect to reaction time and spatial reactivity distribution. An early phase of an unspecific roughness evolution is followed by an advanced phase characterized by a circular degradation pattern, consisting of shallow pits that are steadily renewed over time. The data suggest a hindrance of degradation during the initial roughening process, demonstrating the potential role of targeted surface modification in the large-scale treatment of plastic waste.

npj Materials Degradation (2022)6:93 | <https://doi.org/10.1038/s41529-022-00305-6>

INTRODUCTION

Poly(ethylene terephthalate) (PET) is a versatile thermoplastic with extensive use as packaging material for food and beverage products or as synthetic fibre in the textile industry. The linear polymer chain is composed of terephthalic acid and ethylene glycol units, connected via ester bonds that make the macromolecules sufficiently reactive for different tertiary recycling options; a tremendous advantage over the inert representatives of the “big five” plastics. Mechanical recycling can generally be considered as downcycling^{1,2}, terminated by incineration or landfill. Thus, fossil fuel is eventually converted into CO₂, thereby disturbing the natural carbon cycle³. By contrast, depolymerization and recovery of the monomers allow for closed-loop recycling. Various chemical recycling strategies for PET have been elaborated, but high process costs, mainly due to high-energy consumption and usage of expensive (and harmful) chemicals, still limit the practicability of these technologies⁴.

A recent approach for tertiary PET recycling is bio-based enzymatic hydrolysis, receiving growing attention because it is a sustainable pathway with reduced energy consumption and low greenhouse gas emissions⁵. Compared to chemo-catalytic approaches, the reaction conditions are rather mild, typically in a range of 50–70 °C under atmospheric pressure. At the so-called glass transition temperature (60–75 °C in aqueous solution⁶), the chain flexibility of amorphous PET is significantly increased, facilitating the enzymatic attack. Therefore, the thermostability of the biocatalyst is a prerequisite for efficient depolymerization. Polyester-hydrolyzing enzymes (PHE) have been isolated from a variety of different bacteria and fungi⁷. In their natural habitat, the host organisms probably use these α/β -hydrolases to degrade natural polyesters⁸. A classical chymotrypsin-like Ser-Asp-His triad cleaves the ester bonds in a hydrolysis reaction releasing mainly terephthalic acid, ethylene glycol, and monohydroxyethyl terephthalate⁹. Initially, rather low reaction rates precluded a practical use of enzyme-based PET recycling. After almost two decades of extensive research, more efficient enzyme candidates

have been isolated, especially from thermophilic actinomycetes and metagenomes^{10–13}. Meanwhile, full degradation can be achieved within a few days or even hours^{13–16}. For comparison, the lifetimes of PET in the environment are estimated at 10¹–10² years^{17–19}. We recently isolated and characterized a metagenomic-derived PHE, designated PHL7, which was found to surpass the degradation rates of previously tested enzymes considerably¹³. So far, biaxially stretched (semi-crystalline) PET as used for beverage bottles seems to be unsusceptible to enzyme-mediated degradation in dilute aqueous solutions^{7,13,20}. However, under conditions closer to the natural environment of enzymes, i.e., at high concentrations and very low liquid/solid ratios (moist-solid reaction mixtures), high degradation yields were achieved even for crystalline PET, notably at temperatures well below the glass transition point²¹. Biocatalysts such as PHL7 can be employed as templates for protein engineering to optimize performance.

Aside from the structural–chemical properties of enzyme and substrate, the morphological surface characteristics of the polymer have been recognized to be a key factor controlling degradation rates^{22,23}, but to date, there are only few studies on topographic features evolving during enzymatic degradation of plastic materials. Atomic force microscopy (AFM) and scanning electron microscopy (SEM) have been applied for surface analysis of polyethylene and poly(ethylene vinyl alcohol) blended with starch, showing a formation of cavities as a result of preferred biodegradation of the polysaccharide^{24,25}. An occurrence of sponge-like surface structures during enzymatic treatment was, however, also observed for PET as a homogeneous polymer^{6,26}. Recently, the authors of the present study used vertical scanning interferometry (VSI) and confocal microscopy (CM) to acquire quantitative 3D information on surface retreat and topography during the degradation of amorphous PET, using a high-purity standard material¹³. Indications of possible interrelations between retreat rate and surface morphology were obtained, provoking more in-depth investigations at denser observation intervals, with

¹Helmholtz Centre Dresden-Rossendorf, Institute of Resource Ecology (Research Site Leipzig), Permoserstr. 15, 04318 Leipzig, Germany. ²Leipzig University, Institute of Analytical Chemistry, Linnéstr. 3, 04103 Leipzig, Germany. ✉email: h.lippold@hzdr.de

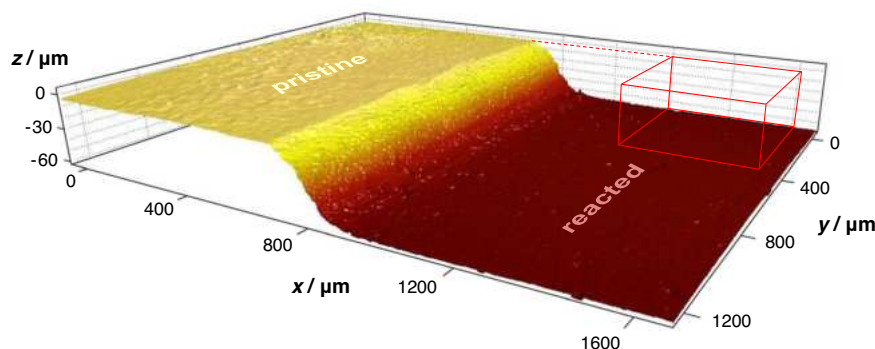


Fig. 1 3D VSI image of a partly reacted PET film surface. The step profile shows the surface retreat after a reaction time of 8 h relative to a protected area (left). For specifying the rate of degradation over time, the volume loss on a unit area (red cuboid) near the protected region was determined.

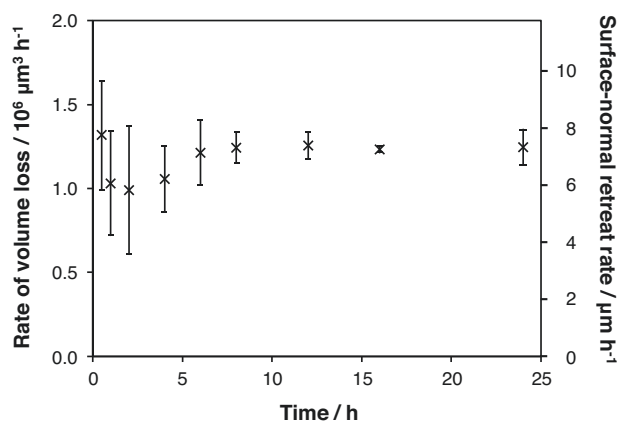


Fig. 2 Rates of volume loss and surface-normal retreat as a function of reaction time. The volumes refer to a basal area of $412 \mu\text{m} \times 412 \mu\text{m}$. Data are given as mean values \pm standard deviations for three independent experiments per time of treatment.

a focus on the initial stage of exposure. As previously, we used the hydrolase PHL7 as a biocatalyst.

Surface-sensitive methods such as VSI and CM, capable of resolving height differences in the lower nm range, are valuable tools for obtaining mechanistic and quantitatively reliable information on degradation rates of materials. This is far beyond bulk volume loss data, e.g., via concentration changes in solutions during dissolution reactions. Surface difference measurements based on repeating topography analyses of materials undergoing degradation can be used to identify highly reactive or locally inert surface sections²⁷. This has led to the use of rate maps in corrosion or dissolution reactions. In addition to visualization in maps, the frequency distributions of rate components can also be quantified in the form of so-called rate spectra^{28,29}. Mechanistically, this reflects the response of the reacting system to the range of activation energies that vary locally across the fluid–solid interface, e.g., due to specific defect types and their spatial density^{30,31}. If the lateral variation of surface retreat is significantly larger than the roughness of the starting material, the resulting topography itself can be used to characterize, as a first approximation, the heterogeneity of the reaction rate. We use this strategy in the present work to analyse not only the mean degradation rate via the mean surface-normal retreat, but also the local surface reactivity via the heterogeneous surface roughness evolution. Following this approach, we can employ the local fluctuation of material degradation to specify the range of reactivity and to evaluate its steady-state behaviour over time.

RESULTS

Global retreat rates

To determine degradation rates, height differences relative to a protected surface area were measured by VSI after reaction with the enzyme for different time periods. An example of the obtained step images is shown in Fig. 1. (A compilation for all reaction times is provided in Supplementary Fig. 1.) Globally, the degradation process appears to be very uniform across the exposed area, leaving a surface parallel to the unreacted part.

In order to quantify the material loss without data reduction by averaging, we extracted the removed volume on a unit area, thus including the full topographic details of the reacted surface. The average rates of degradation, referring to the total reaction time, are plotted in Fig. 2. (The data set is available in Supplementary Table 1.)

For longer reaction times, the rates proved to be quite invariant, whereas the rates for reaction times from 1 to 4 h deviate from this constancy. In spite of substantial variations between individual samples, it appears that degradation is impeded to some degree at this initial stage. Nevertheless, all rate values exceed those hitherto reported for other polyester hydrolases¹³.

Morphological characteristics and heterogeneous reactivity evolving during degradation

In the light of the peculiarities observed for the degradation rates over time, the development of topographic features on the exposed surface part was analysed in detail at higher z resolution. First, the focus was set on the early phase of retreat. In Fig. 3, 3D maps (of unit areas as underlying Fig. 2) are arranged at real depths on a unified z scale.

The pristine surface (0 h) is characterized by an overall smoothness typical of amorphous polymers. It exhibits minor elevations of $<0.5 \mu\text{m}$ with diameters of $\sim 0.1 \text{ mm}$. This wavy topography is still present after a reaction time of 0.5 h when $3 \mu\text{m}$ of the material has been carried away. At the same time, a general roughness has developed. As degradation proceeds, the elevations are more and more eliminated within this unspecific roughening. Still discernible after 1 h, they are completely overridden after 2 h of exposure.

The further morphological evolution can be seen from the 2D images compiled in Fig. 4. The initial roughening process (0–2 h) leaves a surface that may be termed homogeneous at this scale. This is, however, not the final state but the starting point of a second stage: After 4 h, the surface is interspersed with pits, circular in shape and large in diameter compared to the hill-and-dale structure of the roughened base surface.

High-resolution images make visible that the first pits are formed after 2 h already (Fig. 5a). After 4 h, the entire surface is covered by these dish-like craters (Fig. 5b), leaving no remains of

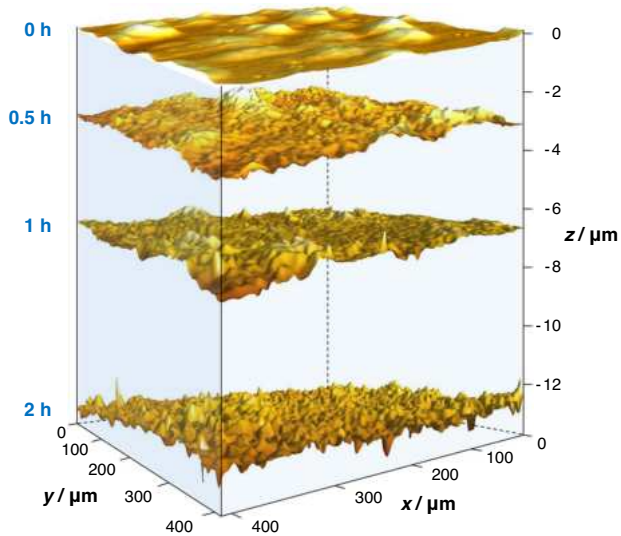


Fig. 3 3D visualization of the initial phase of degradation. The stacked VSI maps show an unspecific roughening process, eliminating a hilly topography present at the beginning.

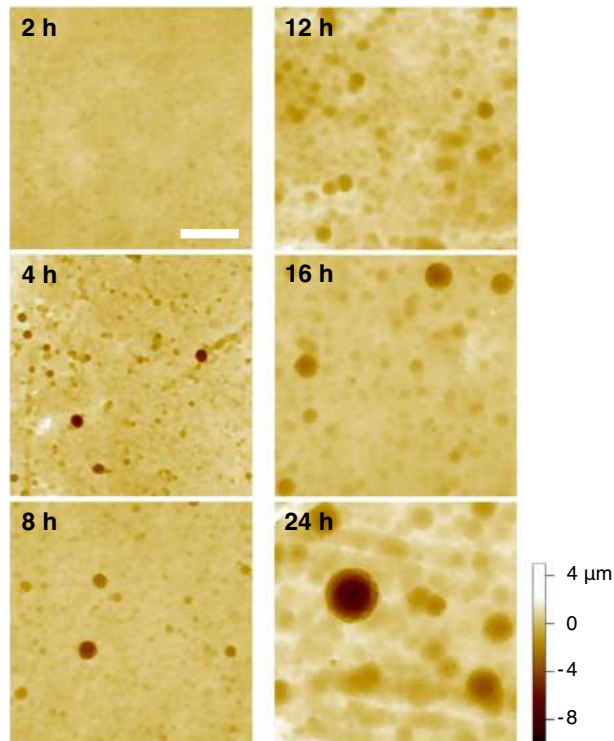


Fig. 4 2D VSI maps showing the evolution of surface topography for reaction times from 2 to 24 h. This advanced degradation phase is characterized by the formation of circular pits. (The scale bar is 100 μm . The z scale is set to zero for the respective modal value of the height distribution.)

the rough background structure generated in the initial phase. Note that the 3D maps are exaggerated in the z -direction. In fact, the pits are very shallow (ratio of depth/diameter = 0.05–0.10), hardly exceeding the basic roughness that dominates after 2 h.

This specific degradation pattern does not change significantly with increasing reaction time (Fig. 4), suggesting a steady-state behaviour. Only for the latest time period (16–24 h), lateral growth of the pits is visible. The same applies to the vertical extension, as

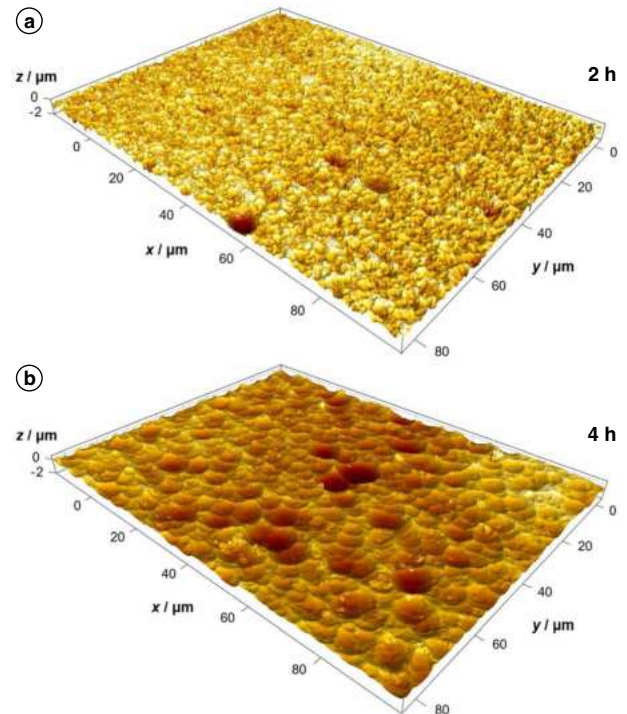


Fig. 5 High-resolution images of PET films after reaction times of 2 and 4 h. The maps were recorded by confocal microscopy. **a** Topography after 2 h, capturing the first occurrence of individual craters. **b** Topography after 4 h, showing complete coverage by craters.

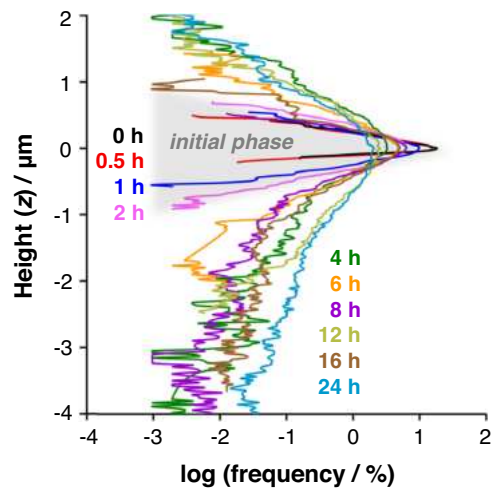


Fig. 6 Histograms of height distributions for PET film surfaces after reaction times from 0 to 24 h. With the height mode centred to zero, positive and negative z values represent hills and dales, respectively. The semi-logarithmic plots display the evolution of high-reactivity centres (tailing towards lower z values) in the advanced degradation phase.

can be taken from the height histograms shown in Fig. 6. Here, the z positions were centred to the maximum frequency after subtracting the modal value of the total retreat. For a sound statistic comparison, the class intervals were unified, and global tilts or bowings were removed beforehand where necessary. (A corresponding analysis for a larger reference area is shown in Supplementary Fig. 2, together with the respective 2D VSI maps.)

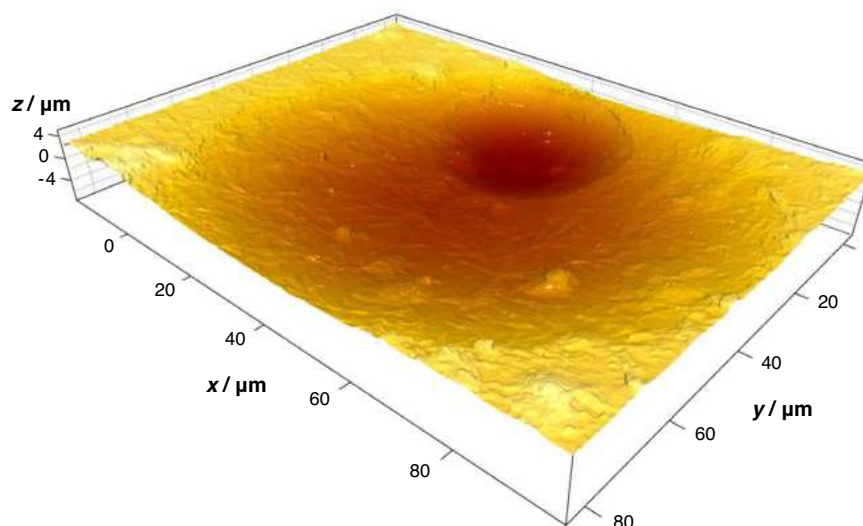


Fig. 7 High-resolution surface detail of a PET film reacted for 24 h. This CM image demonstrates how the crater-type surface is steadily reproduced by the formation of new pits within fading pits of a former generation.

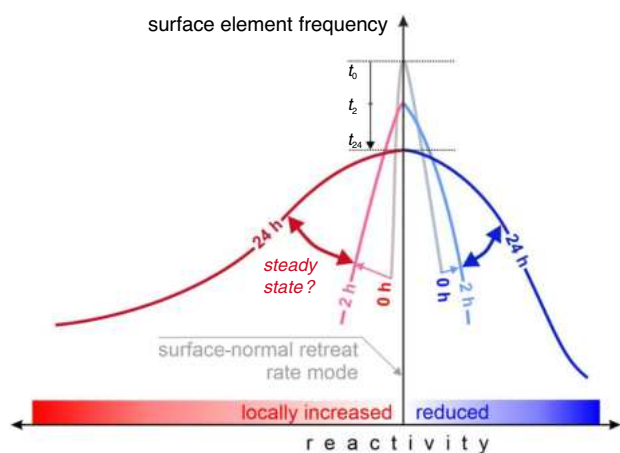


Fig. 8 Generalized depiction of the height evolution of the reacting surfaces during degradation. The height histogram is converted into a representation of surface reactivity. Locally excessive height loss (left, red) represents locally increased surface reactivity. Analogous is the representation on the right (blue). After an initial increase in the reactivity range, a steady state is probably reached after about 2 h, which is reported until 24 h of degradation.

From the histogram plots, the presence of two degradation stages is evident. A clear distinction can be made between the initial phase, where a symmetric distribution is built up, and the advanced phase, where the histograms are negatively skewed to a considerable degree. The distribution width remains within a range of $\Delta z \sim 6 \mu\text{m}$, even for the longest reaction time with a total retreat of $176 \mu\text{m}$ (cf. Supplementary Fig. 1). Hence, the advancement of surface degradation is not to be understood as a proceeding excavation in a sense that craters, once formed, are more and more deepened. Instead, the degradation pattern seems to be in a steady state of continuous renewal, where craters appear and disappear permanently across the surface. Growing in diameter, the pits remain shallow and form the basis of new pits. This mechanism is captured in Fig. 7. Apparently, a certain aspect ratio (depth/diameter) cannot be exceeded.

DISCUSSION

Figure 8 summarizes the detailed observations (as displayed in Fig. 6) in a generalized manner, considering the underlying variations in reactivity. The height histogram shows the frequency of equal height components of the investigated surfaces. For all degradation times, the reference point is the most frequent surface height. In terms of reactivity, it is the most frequent rate of retreat for the respective reaction time.

The existence and increase in the frequency of surface elements with lower height (left) represent an increase in local surface reactivity. Similarly, for the right side of the diagram, this represents a decrease in local surface reactivity. However, this is not a monotonous development: A symmetric broadening until a degradation time of 2 h is followed by an asymmetric spreading for the long-term period until 24 h, but no clear trend for the overall reactivity distribution is evident here. Locally, both increases and decreases in reactivity occur, without exceeding a maximum value. Thus, a steady state-like situation is possible for reaction times greater than ~ 2 h. The sustained variability of reactivity over an extended time period is remarkable, considering that every surface element inherits temporal variations in the local retreat rate that accumulate over time.

The mechanistic background of this circular reactivity pattern is far from obvious. Is it caused by preceding mechanical stress on the surface? Are there heterogeneities in the composition or structure of the plastics? Or is it rather a geometric, self-organized effect of the plastic–enzyme–medium system, reflecting local saturation differences in the degradation process? Looking at the occurrence of circular humps on the pristine surface, one might infer that the cratering is preshaped by an inherent globular texture. However, the pits are distinctly smaller, and as the first of them appear, all traces of the elevated entities have been erased by the initial homogenization of the surface.

Another potential source of heterogeneous reactivity arises from the fact that only flexible polymer chains are accessible to hydrolase enzymes while crystalline domains are deemed to remain unattacked^{1,15,20,32–37}. The applied standard PET material is characterized by a very low degree of crystallinity^{6,11,20,26,37}, visible from complete degradation without any persistent residues¹³. A presence of more rigid and less rigid fractions within the amorphous microstructure, entailing lower and higher reactivity, cannot be excluded. The occurrence of rigid domains is, however, restricted to the vicinity of crystalline units²⁶. Their low abundance does not account for the relative abundance of low-reactivity

components (Figs. 6 and 8), and the circular shape of the high-reactivity regions is hardly explained by this reasoning. Furthermore, it is not comprehensible why such differences in chain mobility do not occur in the upper microns of the PET film, where an unspecific rate distribution was observed.

Similar corrosion pits were recently found on deep sea samples of polyethylene plastics³⁸. In view of the comparable dimensions, the authors ascribed the pits to microbes producing imprints of enzymatic activity, which is, however, not a possible explanation here.

Although crater-like degradation patterns are obviously not restricted to the material under study, we emphasize that quantitative aspects of our findings specifically refer to high-purity amorphous PET. Similar cratering was observed for postconsumer PET packaging after enzymatic or microbial treatment^{26,39}. While degradation rates are comparable^{16,40}, such “real-world” amorphous PET is characterized by inhomogeneities and impurities depending on the individual history of the material, probably resulting in local zones of lower degradation. The occurrence of sponge-like patterns is, however, not a result of impurities, as this study shows. Apparently, it reflects a general mechanism that applies to both homogeneous and more complex materials.

The mechanism itself remains so far unexplained. First of all, it must be clarified whether it is primarily related to material properties or whether it is a specific feature of the enzymatic reaction. In any case, for a generalization and reliable prediction of polymer degradation, we conclude that special attention should be paid to the heterogeneous surface reactivity in future studies. Vertical scanning interferometry and confocal microscopy proved to be very suitable techniques for the detailed monitoring of polymer degradation in space and time. In this way, different stages in the morphological development were identified and characterized as an expression of variations in the spatial reactivity distribution. Importantly, there are indications that this “second-order” rate distribution (Fig. 8) is correlated with the “first-order” rate of total retreat (Fig. 2). Enzymatic degradation of surfaces with a fine roughness as generated during the initial phase appears to be more complicated than degradation of smoother surfaces as present before treatment and in the advanced phase, where the mechanism of the retreat was unveiled to be a continuous reproduction of shallow pits. Process-related questions (e.g., concerning the background of this heterogeneous surface reactivity) need to be addressed in order to provide a fully mechanistic and quantitative explanation of the degradation behaviour. Moreover, these questions are important for large-scale applications of degradation and their calculable prediction. Not least, the answers can open up ways for an acceleration of the process by targeted surface modification.

METHODS

Sample preparation and enzymatic reaction

Amorphous PET film (ES301445, 0.25 mm, Goodfellow GmbH, Germany) was cut into coupons of 2.3 cm × 0.5 cm. After cleaning by sequential washing with 0.5% SDS, water, and 70% ethanol, the coupons were fixed on glass support (2.6 cm × 0.7 cm) with epoxy resin (see Supplementary Fig. 3) and were partially masked with PTFE tape, leaving an accessible PET area of 1.5 cm × 0.5 cm. The degradation reaction was performed in 1.8 mL of 1 M potassium phosphate/NaOH buffer (pH 8) with 27.9 μg mL⁻¹ of the polyester hydrolase PHL7. Production and purification of PHL7 were carried out as described previously¹³. The PET film samples were reacted at 70 °C while shaking at 700 rpm for 0.5, 1, 2, 4, 6, 8, 12, 16, and 24 h (individual samples for each time period). The reaction was stopped by removing the supernatant and washing the samples sequentially with water, 0.5% SDS, water, and 70% ethanol.

Surface topography analysis

Height distributions of PET film surfaces were acquired by means of an S neox 3D optical profiler (Sensofar Metrology, Spain), operated in both VSI white-light mode using a ×10 Mirau objective (Nikon) and in the mode of scanning microdisplay confocal microscopy (CM) using a ×150 confocal objective (Nikon). In brief, the z position of a distance criterion (VSI: equal interferometric path lengths, CM: optical focus) is determined for every x, y position, based on the light intensities recorded by a CCD camera in a piezo-driven height scan. The fields of view are 1754 μm × 1321 μm for the ×10 objective and 117 μm × 88 μm for the ×150 objective, with pixel sizes of 1.3 μm × 1.3 μm and 0.09 μm × 0.09 μm, respectively. Vertical resolutions achieved are ~1 nm in the VSI mode and ~10 nm in the CM mode. Visualization and data processing were performed using the software SPIP (version 6.7.4, Image Metrology, Denmark).

DATA AVAILABILITY

The raw/processed data that support the findings of this study are available from the corresponding author upon reasonable request.

Received: 27 June 2022; Accepted: 2 November 2022;

Published online: 12 November 2022

REFERENCES

- Badia, J. D., Strömberg, E., Karlsson, S. & Ribes-Greus, A. The role of crystalline, mobile amorphous and rigid amorphous fractions in the performance of recycled poly (ethylene terephthalate) (PET). *Polym. Degrad. Stabil.* **97**, 98–107 (2012).
- Schyns, Z. O. G. & Shaver, M. P. Mechanical recycling of packaging plastics: a review. *Macromol. Rapid Commun.* **42**, e2000415 (2021).
- Dhaka, V. et al. Occurrence, toxicity and remediation of polyethylene terephthalate plastics. A review. *Environ. Chem. Lett.* **20**, 1777–1800 (2022).
- Damayanti, D. & Wu, H.-S. Strategic possibility routes of recycled PET. *Polymers* **13**, 1475 (2021).
- Singh, A. et al. Techno-economic, life-cycle, and socioeconomic impact analysis of enzymatic recycling of poly(ethylene terephthalate). *Joule* **5**, 2479–2503 (2021).
- Thomsen, T. B., Hunt, C. J. & Meyer, A. S. Influence of substrate crystallinity and glass transition temperature on enzymatic degradation of polyethylene terephthalate (PET). *N. Biotechnol.* **69**, 28–35 (2022).
- Kawai, F., Kawabata, T. & Oda, M. Current knowledge on enzymatic PET degradation and its possible application to waste stream management and other fields. *Appl. Microbiol. Biotechnol.* **103**, 4253–4268 (2019).
- Chen, S., Su, L., Chen, J. & Wu, J. Cutinase: characteristics, preparation, and application. *Biotechnol. Adv.* **31**, 1754–1767 (2013).
- Roth, C. et al. Structural and functional studies on a thermostable polyethylene terephthalate degrading hydrolase from *Thermobifida fusca*. *Appl. Microbiol. Biotechnol.* **98**, 7815–7823 (2014).
- Sulaiman, S. et al. Isolation of a novel cutinase homolog with polyethylene terephthalate-degrading activity from leaf-branch compost by using a metagenomic approach. *Appl. Environ. Microb.* **78**, 1556–1562 (2012).
- Kawai, F. et al. A novel Ca²⁺-activated, thermostabilized polyesterase capable of hydrolyzing polyethylene terephthalate from *Saccharomonospora viridis* AHK 190. *Appl. Microbiol. Biotechnol.* **98**, 10053–10064 (2014).
- Xi, X. et al. Secretory expression in *Bacillus subtilis* and biochemical characterization of a highly thermostable polyethylene terephthalate hydrolase from bacterium HR29. *Enzym. Microb. Tech.* **143**, 109715 (2021).
- Sonnendecker, C. et al. Low carbon footprint recycling of post-consumer PET plastic with a metagenomic polyester hydrolase. *ChemSusChem* **15**, e202101062 (2022).
- Müller, R.-J., Schrader, H., Profe, J., Dresler, K. & Deckwer, W.-D. Enzymatic degradation of poly(ethylene terephthalate): rapid hydrolyse using a hydrolase from *T. fusca*. *Macromol. Rapid Comm.* **26**, 1400–1405 (2005).
- Tournier, V. et al. An engineered PET depolymerase to break down and recycle plastic bottles. *Nature* **580**, 216–219 (2020).
- Lu, H. et al. Machine learning-aided engineering of hydrolases for PET depolymerization. *Nature* **604**, 662–667 (2022).

17. Allen, N. S., Edge, M. & Mohammadian, M. Physicochemical aspects of the environmental degradation of poly(ethylene terephthalate). *Polym. Degrad. Stabil.* **43**, 229–237 (1994).
18. Müller, R.-J., Kleeberg, I. & Deckwer, W.-D. Biodegradation of polyesters containing aromatic constituents. *J. Biotechnol.* **86**, 87–95 (2001).
19. Ioakeimidis, C. et al. The degradation potential of PET bottles in the marine environment: an ATR-FTIR based approach. *Sci. Rep.* **6**, 23501 (2016).
20. Ronkvist, Å. M., Xie, W., Lu, W. & Gross, R. A. Cutinase-catalyzed hydrolysis of poly(ethylene terephthalate). *Macromolecules* **42**, 5128–5138 (2009).
21. Kaabel, S. et al. Enzymatic depolymerization of highly crystalline polyethylene terephthalate enabled in moist-solid reaction mixtures. *Proc. Natl Acad. Sci. USA* **118**, e2026452118 (2021).
22. Mohanan, N., Montazer, Z., Sharma, P. K. & Levin, D. B. Microbial and enzymatic degradation of synthetic plastics. *Front. Microbiol.* **11**, 580709 (2020).
23. Chamas, A. et al. Degradation rates of plastics in the environment. *ACS Sustain. Chem. Eng.* **8**, 3494–3511 (2020).
24. Araújo, M. A., Cunha, A. M. & Mota, M. Changes on surface morphology of corn starch blend films. *J. Biomed. Mater. Res. A* **94**, 720–729 (2010).
25. Vieyra, H., Aguilar-Méndez, M. A., & San Martín-Martínez, E. Study of biodegradation evolution during composting of polyethylene–starch blends using scanning electron microscopy. *J. Appl. Polym. Sci.* **127**, 845–853 (2013).
26. Wei, R. et al. Biocatalytic degradation efficiency of postconsumer polyethylene terephthalate packaging determined by their polymer microstructures. *Adv. Sci.* **6**, 1900491 (2019).
27. Fischer, C. & Luttge, A. Pulsating dissolution of crystalline matter. *Proc. Natl Acad. Sci. USA* **115**, 897–902 (2018).
28. Fischer, C., Arvidson, R. S. & Luttge, A. How predictable are dissolution rates of crystalline material? *Geochim. Cosmochim. Acta* **98**, 177–185 (2012).
29. Fischer, C., Finkeldei, S., Brandt, F., Bosbach, D. & Luttge, A. Direct measurement of surface dissolution rates in potential nuclear waste forms: The example of pyrochlore. *ACS Appl. Mater. Interfaces* **7**, 17857–17865 (2015).
30. Fischer, C. & Luttge, A. Beyond the conventional understanding of water–rock reactivity. *Earth Planet. Sci. Lett.* **457**, 100–105 (2017).
31. Bollermann, T. & Fischer, C. Temporal evolution of dissolution kinetics of poly-crystalline calcite. *Am. J. Sci.* **320**, 53–71 (2020).
32. Marten, E., Müller, R.-J. & Deckwer, W.-D. Studies on the enzymatic hydrolysis of polyesters. II. Aliphatic–aromatic copolyesters. *Polym. Degrad. Stabil.* **88**, 371–381 (2005).
33. Vertommen, M. A. M. E., Nierstrasz, V. A., van der Veer, M. & Warmoeskerken, M. M. C. G. Enzymatic surface modification of poly(ethylene terephthalate). *J. Biotechnol.* **120**, 376–386 (2005).
34. Brueckner, T., Eberl, A., Heumann, S., Rabe, M. & Guebitz, G. M. Enzymatic and chemical hydrolysis of poly(ethylene terephthalate) fabrics. *J. Polym. Sci. Pol. Chem.* **46**, 6435–6443 (2008).
35. Donelli, I., Freddi, G., Nierstrasz, V. A. & Taddei, P. Surface structure and properties of poly(ethylene terephthalate) hydrolyzed by alkali and cutinase. *Polym. Degrad. Stabil.* **95**, 1542–1550 (2010).
36. Gamerith, C. et al. Enzymatic recovery of polyester building blocks from polymer blends. *Process. Biochem.* **59**, 58–64 (2017).
37. Oda, M. et al. Enzymatic hydrolysis of PET: functional roles of three Ca²⁺ ions bound to a cutinase-like enzyme, Cut190*, and its engineering for improved activity. *Appl. Microbiol. Biotechnol.* **102**, 10067–10077 (2018).
38. Zhang, X. & Peng, X. How long for plastics to decompose in the deep sea? *Geochem. Perspect. Lett.* **22**, 20–25 (2022).
39. Yoshida, S. et al. A bacterium that degrades and assimilates poly(ethylene terephthalate). *Science* **351**, 1196–1199 (2016).
40. Frank, R., Krinke, D., Sonnendecker, C., Zimmermann, W. & Jahnke, H.-G. Real-time noninvasive analysis of biocatalytic PET degradation. *ACS Catal.* **12**, 25–35 (2022).

ACKNOWLEDGEMENTS

This work received funding from Sächsisches Staatsministerium für Wissenschaft, Kultur und Tourismus (project No. 100387903) in the framework of the ERA CoBioTech project MIPLACE. The authors would like to thank Prof. Klaus Kroy and Prof. Wolfgang Zimmermann for their valuable discussions. Technical support by Ziyue Zhao is gratefully acknowledged.

AUTHOR CONTRIBUTIONS

H.L., C.F. and C.S. wrote the manuscript. L.K. and C.S. performed the degradation experiments. L.K. and H.L. conducted the surface-analytical measurements. H.L. and C.F. analysed and visualized the data. C.F., C.S. and J.M. conceptualized the methodology and supervised the investigations.

FUNDING

Open Access funding enabled and organized by Projekt DEAL.

COMPETING INTERESTS

The authors declare no competing interests.

ADDITIONAL INFORMATION

Supplementary information The online version contains supplementary material available at <https://doi.org/10.1038/s41529-022-00305-6>.

Correspondence and requests for materials should be addressed to Holger Lippold.

Reprints and permission information is available at <http://www.nature.com/reprints>

Publisher's note Springer Nature remains neutral with regard to jurisdictional claims in published maps and institutional affiliations.



Open Access This article is licensed under a Creative Commons Attribution 4.0 International License, which permits use, sharing, adaptation, distribution and reproduction in any medium or format, as long as you give appropriate credit to the original author(s) and the source, provide a link to the Creative Commons license, and indicate if changes were made. The images or other third party material in this article are included in the article's Creative Commons license, unless indicated otherwise in a credit line to the material. If material is not included in the article's Creative Commons license and your intended use is not permitted by statutory regulation or exceeds the permitted use, you will need to obtain permission directly from the copyright holder. To view a copy of this license, visit <http://creativecommons.org/licenses/by/4.0/>.

© The Author(s) 2022